Open Access

Recent Progress in Science and Engineering

LIDSEN Publishing Inc.

Review

Performance Enhancement of CIGS Thin-Film Solar Cells through Numerical Modeling

Damir Istamov [1, †, *], Asliddin Komilov [2, †]

1. Physical-Technical Institute of Uzbekistan Academy of Sciences 2B Chingiz Aytmatov Street, 100084 Tashkent, Uzbekistan; E-Mail: istamov@uzsci.net
2. National Research Institute of Renewable Energy Sources, 2B Chingiz Aytmatov Street, 100084 Tashkent, Uzbekistan; E-Mail: asliddin@rambler.ru

† These authors contributed equally to this work.

* **Correspondence:** Damir Istamov; E-Mail: istamov@uzsci.net

Academic Editor: Orlando Corigliano

Recent Prog Sci Eng
2026, volume 2, issue 2
doi:10.21926/rpse.2602011

Received: March 04, 2026
Accepted: June 01, 2026
Published: June 16, 2026

Abstract

Copper indium gallium selenide (CIGS) thin-film solar cells remain among the most promising photovoltaic technologies due to their high absorption coefficient, tunable bandgap, and compatibility with low-temperature processing. This manuscript presents a comprehensive numerical investigation of performance enhancement strategies for CIGS-based solar cells using one-dimensional and multidimensional simulation frameworks. Device optimization is analyzed by systematically varying absorber composition, bandgap grading, defect density, and doping concentration, as well as through engineering of buffer, window, and back-surface-field (BSF) layers. SCAPS-1D simulations are employed to evaluate steady-state optoelectronic behavior. At the same time, advanced TCAD tools such as Silvaco Atlas and Synopsys Sentaurus provide spatially resolved insight into heterojunction band alignment, interface recombination, and module-level effects including laser scribing. The impact of alkali post-deposition treatments, grain-boundary passivation, tuning of the conduction-band offset, and alternative non-toxic buffer materials is assessed. Advanced architectures—including double-absorber layers, multi-junction stacks, bifacial designs, and perovskite/CIGS

tandems—are examined to identify pathways beyond single-junction efficiency limits. The results indicate that coordinated optimization of composition gradients, carrier-selective contacts, and interface passivation can enable power conversion efficiencies exceeding 30% in numerical simulations under idealized conditions. However, these values represent theoretical upper bounds, while experimentally certified efficiencies remain significantly lower, underscoring the importance of incorporating realistic material properties and recombination mechanisms in modeling. Overall, this work highlights the central role of multi-physics simulation in guiding the design and experimental realization of next-generation high-efficiency CIGS solar cells.

Keywords
CIGS thin-film solar cells; numerical modeling; SCAPS-1D; TCAD simulation; bandgap engineering; buffer layer optimization; back surface field (BSF); post-deposition treatment; multi-junction photovoltaics; tandem solar cells; device optimization

1. Introduction

The global Copper Indium Gallium Selenide (CIGS) photovoltaic market has grown strongly over the last decade [1]. Among various novel semiconductors, CIGS is doubtless one of the most promising materials, performing exceptionally well in terms of carrier lifetime and processability while ensuring high conversion efficiency [2-9]. Numerical modeling and simulation have been employed since the early days of this research field to correlate particular device and material parameters with cell output characteristics [10-14]. Modern simulation tools, such as Atlas of Silvaco, are based on digital-resolution 2D transport equations that govern conduction mechanisms in semiconductor devices [1]. Another widely used tool is the Solar Cell Capacitance Simulator (SCAPS-1D), a well-established numerical tool for modeling thin-film solar cells by solving continuity and electrostatic potential equations in a steady-state environment [15].

CIGS is a direct bandgap chalcopyrite semiconductor with a polycrystalline nature, chemically represented as $Cu(In_{1-x}, Ga_x)Se_2$, where x can vary from 0 to 1 [16, 17]. This tunability allows the bandgap to be easily changed from 1.0 eV to 1.7 eV by increasing the gallium-to-indium ratio of the absorber [18-20]. Effective bandgap engineering can reduce the recombination rate via electric field enhancement, thereby increasing the electron-hole pair production rate [21]. Recent electrical CIGS simulation baseline models have incorporated post-deposition treatment (PDT) effects, such as the use of heavy alkali fluoride compounds like KF, RbF, and CsF, resulting in significant performance improvements [22]. Figure 1, illustrates an updated SCAPS model schematic consisting of the CIGS absorber, a surface defect layer (SDL), a CdS buffer, and window layers of $Zn_{1-x}Mg_xO$ (ZMO) and Al:ZnO (AZO).

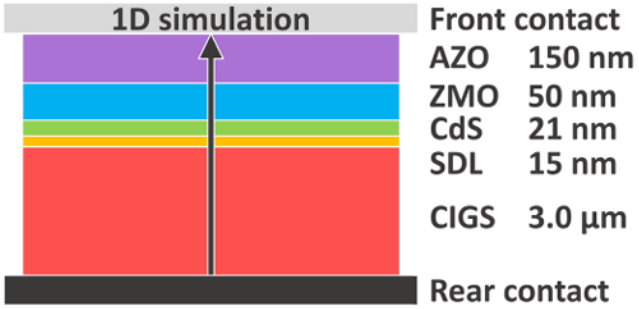

Figure 1 SCAPS model schematic of the CIGS device stack. Approximate layer thicknesses: AZO/ZMO window (~200 nm total), CdS buffer (~25-50 nm), CIGS absorber (~2000-2500 nm), and Mo back contact (~500 nm). SDL = surface defect layer. Adapted from Ref. [22].

To enhance performance, several critical layers and their properties must be optimized. The window layer must be highly transmittable in the visible spectrum while maintaining high electrical conductivity to aid in the collection of photogenerated carriers [23]. The n-type conductivity of materials like ZnO enables effective electron transit, and doping with aluminum (ZnO:Al) increases conductivity to maintain low resistive losses [23]. In addition to traditional window layers, the role of front contacts like Indium Tin Oxide (ITO) has been thoroughly explored using SILVACO ATLAS to achieve ultra-high efficiencies [24]. The buffer layer, such as CdS, contributes to p–n-junction formation and enhances the lattice match between the absorber and window layers [18, 25, 26]. However, to avoid the toxic effects of cadmium, simulations have investigated alternative buffer layers like Zn(O,S) [1] or less toxic Indium Phosphide (InP) [27].

Further performance enhancements are achieved through the implementation of a back surface field (BSF) and rear-surface passivation. Including a BSF layer, such as thin CuInSe, in thin-film cells has a significant impact compared to conventional structures [28]. The introduction of a BSF layer aims to minimize recombination losses by optimizing the band alignment and electric field profile within the device [29]. Recent studies have reported the use of Sb_2S_3 as a back-surface field (BSF) layer, achieving power conversion efficiencies (PCE) above 31% in numerical simulations under idealized conditions, in which recombination losses are significantly suppressed and interface properties are optimized [30]. Passivation layers, such as Al_2O_3 at the rear interface, can effectively reduce carrier recombination and improve the open-circuit voltage (V_{OC}) [22].

Advanced architectures, such as tandem solar cells, integrate CIGS with other materials to exceed the efficiency threshold of single-junction PV cells [31]. Perovskite-CIGS tandem cells have demonstrated promise in overcoming these constraints, utilizing a top cell for high-energy photons and a CIGS bottom cell for low-energy photons [31]. Furthermore, innovative designs using double or triple-junction absorber layers, such as CZO/CIGS/CZTS configurations, have increased efficiency from 18.11% to 24.5% due to optimized light absorption and improved charge-carrier dynamics [32].

1.1 Modeling and Multi-Physics Simulation of High-Efficiency CIGS Solar Cells

The development of high-efficiency Cu(In, Ga)Se_2 (CIGS) solar cells requires a robust multi-physics modeling approach to address the complex optoelectronic interactions within thin-film and ultrathin-film architectures. CIGS technology is recognized as one of the most promising options for future thin-film photovoltaics (PV) due to its high absorption coefficient (~10^5 cm^{-1} at 1.4 eV) and a

tunable bandgap that can easily be varied from 1.07 eV up to 1.7 eV by increasing the [Ga]/([Ga] + [In]) ratio [22, 30, 33-35].

2. Numerical Analysis of Photovoltaic Parameters Using SCAPS-1D

This section reviews one-dimensional numerical modeling of CIGS solar cells using SCAPS-1D. Its steady-state, one-dimensional formulation makes SCAPS particularly well-suited for systematic analysis of absorber properties, defect density, and layer thickness optimization. However, SCAPS-1D cannot capture lateral inhomogeneities, grain-boundary effects, or complex interface geometries; these phenomena require multidimensional modeling approaches discussed in Section 3.

Numerical analysis provides insight into PV device operation and enables systematic optimization of parameters such as thickness, doping density, and defect concentration [36]. SCAPS-1D, developed at Ghent University [37], solves the Poisson and carrier continuity equations under steady-state conditions and is widely used for modeling thin-film solar cells [23, 36-38].

2.1 Absorber Layer Engineering and BSF Optimization

Recent SCAPS-based studies indicate that high-efficiency CIGS solar cells are achieved through distinct optimization strategies rather than isolated parameter tuning. BSF engineering, such as Sb_2S_3 (31.15%, [30]) and Cu_2O-based carrier-selective contacts (31.84%, [39]), enhances performance primarily by improving band alignment and suppressing rear-interface recombination [38, 39]. In parallel, window layer optimization reduces optical and resistive losses, directly impacting J_{SC} and FF, while advanced architectures (e.g., double absorbers) improve spectral utilization, reaching efficiencies up to 29.22% [37].

However, these values are obtained under idealized simulation conditions, including negligible defect densities and perfect interface passivation. In contrast, the certified experimental efficiency of CIGS cells remains ~23.35% [40], highlighting a significant gap between theoretical predictions and practical devices. This comparison indicates that interface engineering and recombination control play a more dominant role than absorber scaling alone in achieving high efficiency.

These high efficiencies (>30%) are obtained under idealized simulation conditions, including: (i) perfect interface passivation with near-zero interface defect density; (ii) negligible shunt losses ($R_{sh} \rightarrow \infty$) and optimized series resistance; (iii) ideal optical boundary conditions enabling maximum light absorption; and (iv) carrier mobilities and lifetimes approaching their theoretical limits. Such assumptions significantly suppress recombination and enhance carrier collection, leading to optimistic performance predictions.

In contrast, the current certified experimental efficiency of CIGS solar cells remains ~23.35%, indicating a substantial gap between theoretical simulations and practical device realization. This discrepancy highlights the importance of incorporating realistic material and interface properties in future modeling studies.

2.2 Window Layer and Buffer Layer Optimization

The impact of diverse window layers, such as ZnO, I_2S_3, ITO, AZO, and ZnMgO, has been meticulously investigated in SCAPS-1D [23]. As illustrated in Figure 2. Structure of a CIGS solar cell.

[23]. The window layer must possess strong electrical conductivity and high optical transparency to minimize absorption losses before light reaches the absorber [23]. Furthermore, the introduction of a hole-transport layer (HTL) like NiO can significantly boost efficiency, as evidenced by the increase from 9.89% to 19.55% at 300 K [36].

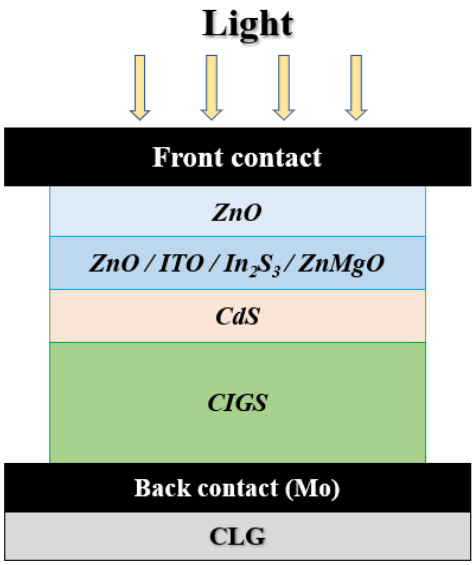

Figure 2 Schematic structure of a typical CIGS solar cell, including the AZO window layer, CdS buffer layer, CIGS absorber, and Mo back contact. The figure illustrates the layer sequence and carrier transport pathways. Adapted from Ref. [23].

2.3 Advanced Architectures: Tandem and Multi-Junction Designs

Tandem architectures, particularly perovskite/CIGS designs, offer a pathway beyond the Shockley-Queisser limit by combining sub-cells with complementary absorption spectra [35, 41]. In a tandem configuration, the CIGS cell serves as an ideal bottom sub-cell due to its stability and ability to capture lower-energy photons transmitted through the top sub-cell, as illustrated in Figure 3 [31].

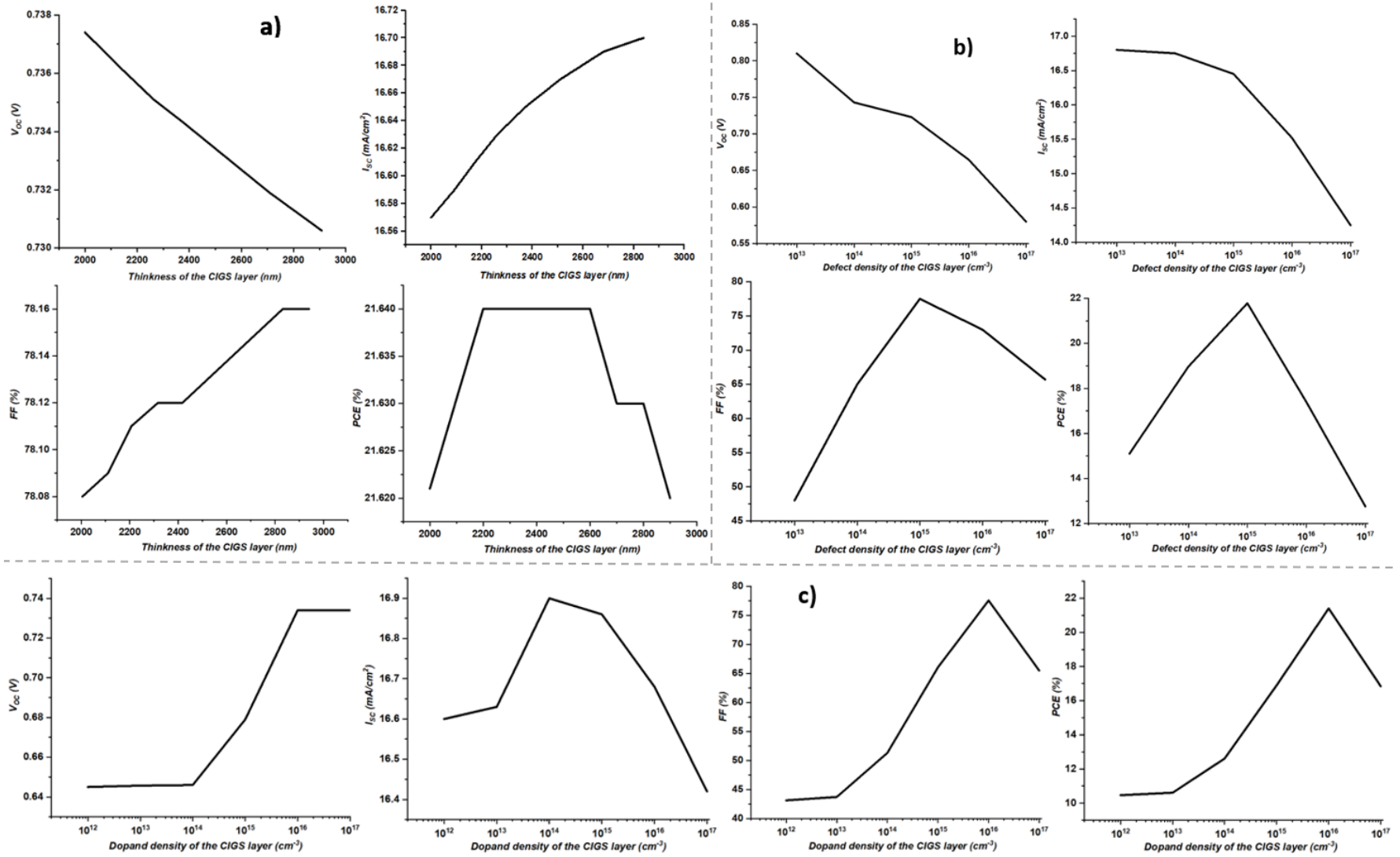

Figure 3 Schematic of a perovskite/CIGS tandem solar cell architecture, showing the top perovskite sub-cell (high-energy photon absorber) and the bottom CIGS sub-cell (low-energy photon absorber) in a two-terminal (2T) monolithic configuration. Adapted from Ref. [31].

The degradation of photovoltaic parameters with increasing defect density is governed by recombination mechanisms. Higher defect density enhances Shockley-Read-Hall recombination, increasing the dark saturation current and reducing V_{OC}. It also shortens carrier lifetimes and diffusion lengths, leading to lower J_{SC}, while increased recombination losses degrade the fill factor (FF).

The double-active-layer approach, in which the absorber is subdivided into layers such as $CIGS_1$ and $CIGS_2$ with different band gaps, has been reported to achieve PCE values up to 29.22% in SCAPS-1D simulations under optimized conditions, including controlled defect density and bandgap grading [37]. These improvements are primarily attributed to enhanced spectral utilization and improved carrier collection efficiency. Optimization parameters used in such high-efficiency simulations are summarized in Table 1.

Table 1 Input specifications for a thin-layered CIGS-based solar cell [38].

Parameters	ZnO:Al	i-ZnO	CdS	CIGS
Thickness (nm)	150	50	40	2500
Bandgap, E_g (eV)	3.37	3.37	2.48	1.27
Dielectric Permittivity, ε_r	8.490	8.490	10.00	13.6
Electron affinity, χ (eV)	4.5	4.5	4.4	4.5
CB EDS, N_C (cm^{-3})	2.20E+18	2.20E+18	2.20E+18	2.20E+18
VB EDS, N_V (cm^{-3})	1.80E+19	1.80E+19	1.80E+19	1.80E+19
Electron mobility, μ_n ($cm^2\ V^{-1}\ s^{-1}$)	1.00E+2	1.10E+2	1.00E+2	1.00E+2

Additional studies report that alternative buffer layers, such as InP, can achieve efficiencies of 28.01% in SCAPS-1D simulations [27], while WS_2/PEDOT:PSS passivation structures yield efficiencies of up to 25.70% under similarly idealized conditions [29].

2.4 Critical Assessment of High-Efficiency Simulation Assumptions

The assumptions underlying high-efficiency SCAPS-1D results can be grouped into four main categories, each of which contributes to an overestimation of the simulated power conversion efficiency (PCE). Table 2 summarizes these assumptions for representative studies reporting PCE ≥ 25% and compares them with experimentally measured parameters from the certified CIGS record [41].

Table 2 Simulation input assumptions for high-efficiency CIGS studies (PCE ≥ 25%) compared with experimentally measured parameters [41].

[Ref]	PCE (%)	$N_{t,\ CIGS}$ (cm^{-3})	$N_{t,\ int}$ (cm^{-2})	R_{sh}; R_s	Optical Model	Key Idealisation
[30]	31.15	~10^{14}	0 (zero)	∞; 0 Ω·cm^2	AM1.5G, no parasitic absorption, ideal ARC	N_t 1-10× below poly-CIGS; zero interface defects; $R_{sh} \rightarrow \infty$; no optical losses. All four idealizations active simultaneously. Represents a theoretical PCE ceiling.
[39]	31.84	~10^{14}	0 (zero)	∞; 0	AM1.5G, ideal ARC	Highest PCE in this review. Gap vs. certified record = 8.49 pp — the largest discrepancy. Carrier μ at single-crystal limit. All loss mechanisms suppressed.
[37]	29.22	~10^{14}-10^{15}	Included (optimised low)	High; not stated	AM1.5G, standard	Two-absorber stack; inter-absorber interface defects optimised, not experimentally validated. Partially idealised; best-case Ga grading assumed.
[27]	28.01	10^{14}-10^{15}	~10^{12} (low)	Varied parametric	AM1.5G, standard	InP/CIGS CBO less experimentally characterised than CdS/ CIGS. Carrier lifetime at bulk theoretical value. Peak PCE uses optimum R_{sh} from sweep.
[23]	25.81-28.14	10^{14}-10^{15}	10^{12}-10^{13} (varied)	Finite; included	AM1.5G, standard	Most realistic parameter set in this review. Lowest simulated PCE; result closest to certified experimental value — consistent with the monotonic PCE-realism relationship.
[40]	23.35	~10^{15}-10^{16} (measured)	~10^{10}-10^{12} (measured)	Finite (measured)	AM1.5G certified, no ARC	Only certified result. All loss mechanisms present: GB recombination, non-uniform defects, parasitic absorption, finite contact recombination. Sets the realistic efficiency target.

(i) Defect density (N_t). Most studies reporting PCE above 29% assume relatively low bulk defect densities (~10^{14} cm^{-3}) and near-zero interface defect densities. In contrast, experimentally measured polycrystalline CIGS absorbers typically exhibit higher defect densities (10^{15}-10^{16} cm^{-3}), which increase recombination losses, reduce carrier lifetime, and limit open-circuit voltage. As a result, simulated efficiencies based on low defect densities represent optimistic upper limits rather than realistic device performance.

(ii) Interface and contact boundary conditions. Many simulation studies assume ideal or unreported contact conditions, effectively neglecting interface recombination at both the front and rear contacts. In real devices, the CdS/CIGS interface and the Mo back contact introduce finite recombination losses that reduce both V_{OC} and carrier collection efficiency. Ignoring these effects leads to systematic overestimation of device performance.

(iii) Optical modeling. Most SCAPS-based studies employ idealized optical conditions, typically assuming full absorption of incident light and neglecting parasitic absorption in the window and buffer layers. Experimental measurements show that these layers absorb part of the incoming spectrum, reducing J_{SC}. The omission of these optical losses contributes to inflated simulated efficiencies.

(iv) Carrier transport parameters. Carrier mobility and lifetime values used in simulations are often close to theoretical limits. However, experimentally measured values in polycrystalline CIGS are lower due to grain-boundary scattering and material inhomogeneity. This discrepancy leads to overestimated carrier collection and fill factor in numerical models.

Taken together, these assumptions result in a cumulative overestimation of PCE in high-efficiency simulations. Notably, the study with the most realistic parameter set (Kakade et al. [23]) yields the lowest simulated efficiency among the reviewed works and is closest to the certified experimental value of 23.35% [40]. This trend indicates that simulated efficiency decreases as modeling assumptions approach physical realism.

Therefore, reported efficiencies exceeding 30% should be interpreted as theoretical upper limits. Bridging the gap between simulation and experiment requires incorporating realistic defect densities, non-ideal interfaces, optical losses, and experimentally validated transport parameters into future modeling studies.

3. Advanced 2D/3D Device Characterization and Design Optimization in TCAD

This section addresses multidimensional device modeling using TCAD tools such as Silvaco Atlas and Synopsys Sentaurus. Unlike SCAPS-1D, TCAD enables 2D and 3D simulations of spatially resolved physical processes, including band-alignment variations, grain-boundary recombination, and module-level effects such as interconnect scribing. This makes TCAD essential for capturing complex device physics beyond the limitations of one-dimensional models.

Advanced Technology Computer-Aided Design (TCAD) tools, such as Silvaco Atlas and Synopsys Sentaurus, provide multi-dimensional insight into device physics that go beyond 1D modeling [1, 16, 21]. These simulators are essential for modeling conduction-band offsets (CBO), interface states, and spatial inhomogeneities [21, 33]. The optimal CBO of +0.5 eV is found to be significant for heterojunction performance [1]. This optimal value corresponds to a spike-like conduction band alignment at the CIGS/CdS interface. This band alignment is illustrated schematically in Figure 4. A small positive (spike) CBO suppresses interface recombination by introducing a barrier for minority

carriers (holes), while still allowing efficient electron transport across the junction. In contrast, a negative (cliff-like) CBO enhances interface recombination, leading to reduced open-circuit voltage and overall device performance.

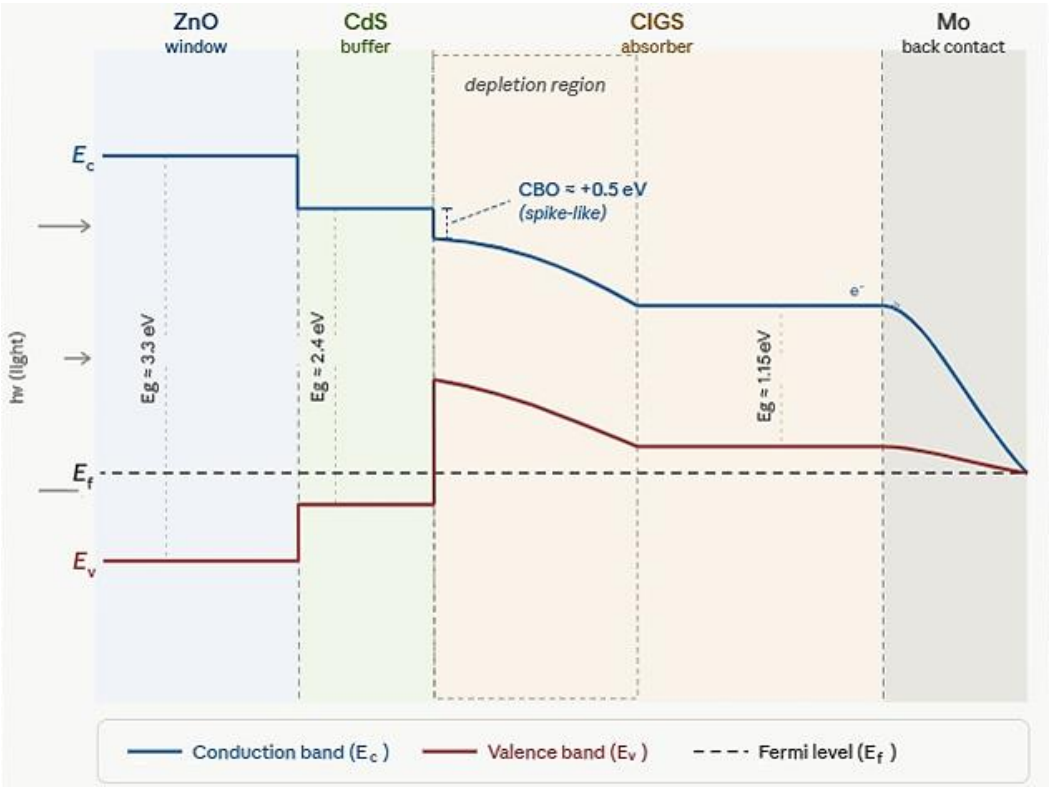

Figure 4 Energy band diagram of the ZnO/CdS/CIGS/Mo solar cell structure, showing the conduction band edge (E_c), valence band edge (E_v), and Fermi level alignment. The diagram illustrates the spike-like conduction band offset (CBO) at the CdS/CIGS interface and the band bending in the depletion region.

Therefore, precise control of band alignment at the buffer/absorber interface is critical for minimizing recombination losses and maximizing device efficiency.

The band alignment illustrated in Figure 4 governs the primary recombination pathway at the buffer/absorber interface and forms the physical basis for CBO optimization studies reviewed throughout this section.

Multi-junction designs simulated in Silvaco TCAD demonstrate significant PCE enhancements: from 18.11% for single-junction CIGS to 21% for double CZO/CIGS, and further to 24.5% for triple CZO/CIGS/CZTS configurations (Table 3) [33]. This multi-layered approach employs the structures shown in Figure 5 to optimize light absorption and charge dynamics. In parallel, the combination of CZTSe and CIGS double absorbers can improve efficiency up to 29.22% while minimizing the cost of expensive indium [42].

Table 3 Comparative CIGS simulation performance data used for model validation [32].

Structure	V_{OC} (V)	I_{SC} (mA/cm^2)	FF (%)	Efficiency (%)
CdS/CIGS	0.74	35.0	81	16.8
ZnO/CdS/CIGS	0.82	34.8	83	17.6
ZnMgO/ZnO/CdS/CIGS	0.83	37.0	85	19.0
AZO/ZnO/CdS/CIGS	0.80	36.5	83.5	18.2
i-ZnO/ZnO/CdS/CIGS	0.8	36.0	82	18.11

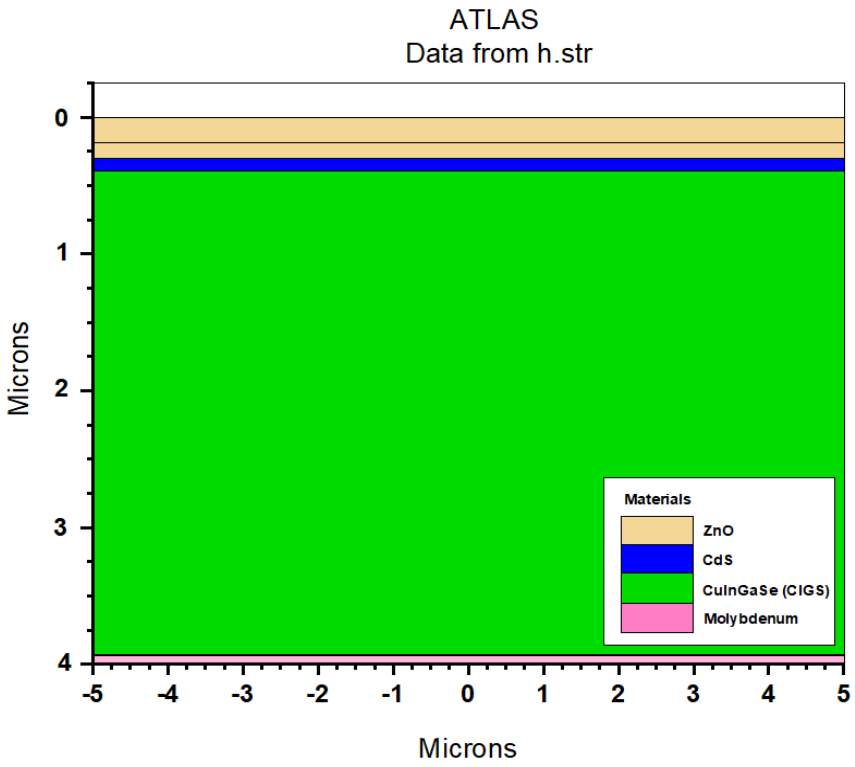

Figure 5 Device architectures simulated in Silvaco TCAD by Hajji et al.: single-junction CIGS (PCE = 18.11%), double-junction CZO/CIGS (PCE = 21%), and triple-junction CZO/CIGS/CZTS (PCE = 24.5%) configurations. Each architecture incorporates an additional absorber layer with a complementary bandgap, enabling sequential photon harvesting across a broader spectral range and yielding progressive PCE enhancement. The ZnO/CdS/CIGS/Mo baseline layer stack is shown for reference. Adapted from Ref. [32].

2D simulations are critical for understanding the behavior of interconnected modules, particularly the impact of laser-patterning scribes (P1, P2, P3) [43]. The P1 scribe separates back electrodes and can introduce a shunt resembling a junction field-effect transistor, in which expanding the space charge region (SCR) into the P1 trench reduces shunt conductance. This behavior is detailed in Figure 6 [44].

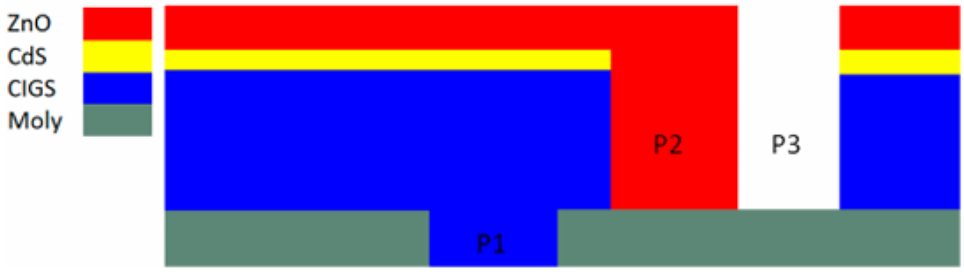

Figure 6 Schematic representation of a CIGS solar module with monolithic interconnection (P1, P2, P3 scribes), illustrating current flow paths and potential shunt formation mechanisms. Adapted from Ref. [44].

The P1-P3 interconnect analysis illustrated in Figure 6 underscores that module-level efficiency losses are intrinsically linked to process precision and shunt geometry, motivating the need for fully calibrated device models. For high-efficiency record cells, such updated baseline models must incorporate post-deposition treatment (PDT) with alkali fluorides, which passivate grain boundaries (GBs) and increase the net free-carrier concentration [22]. The progression of these model updates is depicted in Figure 7, which shows how successive calibration steps — from a basic absorber model to one incorporating SDL, PDT, and electromagnetic optics — progressively close the gap between simulated and certified experimental performance [22]. The N1 signal observed in thermal admittance spectroscopy (TAS) of CIGS devices — historically attributed to deep bulk defects — has been reinterpreted through TCAD back-contact modeling as arising from a transport barrier at the rear Mo/CIGS interface [45].

Figure 7 Progressive refinement of the SCAPS-1D baseline model for ultrathin CIGS solar cells (Violas et al. [22]), illustrating successive calibration steps from a basic single-layer absorber to an advanced structure incorporating: (i) a surface defect layer (SDL) at the CdS/CIGS interface, (ii) post-deposition treatment (PDT) effects of alkali fluoride (KF, RbF, CsF) passivation, and (iii) optical boundary conditions from electromagnetic modeling. Each update narrows the gap between simulated and experimentally certified device parameters (V_{OC}, J_{SC}, FF, PCE), thereby establishing a calibration framework that is transferable to multidimensional TCAD environments. Adapted from Ref. [22].

In the realm of path-finding, co-optimization of composition gradients and buffer layers is critical. Simulations show that thin CdS (10 nm) is preferred for accumulated Ga-profiles, while thicker CdS enhances collection in flatter profiles [46]. Furthermore, the introduction of ITO as a front contact can lead to efficiencies of 23.074% [24].

Bifacial CIGS architectures require transparent rear contacts such as ITO, though these often present an electrical barrier that limits rear-side efficiency [47]. Novel designs like the PMoSe–P architecture-alternating lines of $MoSe_2$ and dielectric-allow for conversion efficiencies surpassing 20% and 15% for front and rear side illumination, respectively [47].

Comprehensive models must also reproduce thermal admittance spectra (TAS) and illumination-dependent I-V-T curves to be considered reliable [48]. As summarized in the following table, experimental and simulated data must align to validate the multi-physics approach.

Finally, the inclusion of time-resolved photoluminescence (TRPL) simulations, as applied to a 1D CIGSe absorber model with linear bandgap grading and shallow defects, enhances the assessment of material quality during production [49].

4. Modeling Challenges and Limitations

Despite significant progress in numerical modeling of CIGS solar cells, several limitations remain that constrain the predictive accuracy of simulation results. First, the polycrystalline nature of CIGS introduces complex grain-boundary (GB) effects that act as both recombination centers and carrier transport pathways. These effects cannot be accurately captured in one-dimensional SCAPS models and require computationally intensive multidimensional approaches.

Second, defect distributions in real devices are inherently non-uniform, whereas most simulations assume spatially homogeneous defect densities. This simplification can lead to discrepancies between simulated and experimental performance. Third, advanced TCAD simulations, particularly in 3D, require substantial computational resources, often limiting the feasibility of large-scale parametric studies.

Furthermore, current models generally neglect coupled thermal and mechanical stress effects, which can influence long-term device stability and degradation. Finally, accurate experimental validation remains challenging due to uncertainties in key input parameters, including defect densities, interface recombination velocities, and material properties. These limitations highlight the need for more physically realistic and experimentally validated modeling frameworks.

5. Conclusions

This study consolidates recent advances in the numerical modeling and structural optimization of CIGS thin-film solar cells. One-dimensional SCAPS-1D simulations effectively capture the influence of absorber thickness, doping density, defect states, and bandgap grading on key photovoltaic parameters. At the same time, multidimensional TCAD analyses provide deeper insights into band alignment, conduction band offsets, grain-boundary effects, and module-level phenomena.

Performance improvements are primarily driven by three coordinated strategies: (i) absorber engineering through compositional grading and defect control, (ii) interface optimization via buffer selection, conduction band alignment, and passivation treatments, and (iii) carrier-selective contact design including advanced window layers and BSF structures. These approaches collectively suppress recombination losses and enhance device performance.

Emerging architectures—including double absorber layers, tandem configurations, and bifacial designs—demonstrate the potential of CIGS technology to surpass conventional single-junction limits. However, efficiencies exceeding 30% are currently achieved only in numerical simulations under idealized conditions, while experimentally certified values remain around ~23.35%, highlighting a significant gap between theoretical predictions and practical realization.

Future progress will likely rely on integrating perovskite/CIGS tandem structures, bifacial thin-film architectures, and AI-assisted multi-parameter optimization frameworks. In parallel, advances in grain-boundary passivation, alkali-treatment strategies, and scalable fabrication of carrier-selective contacts will be essential for translating simulation insights into experimentally viable devices.

Key open challenges remain in accurately modeling defect physics, grain boundary behavior, and interface recombination, as well as in achieving reliable experimental validation of model parameters. Addressing these challenges is critical for bridging the gap between simulation and experiment and for enabling the next generation of high-efficiency, scalable CIGS solar technologies.

Overall, this review highlights that the primary bottleneck in CIGS performance is not optical absorption. Still, the control of recombination mechanisms at interfaces and defects underscores the central role of physically realistic modeling in future device design.

Acknowledgment

This work was carried out within the framework of project AL-9224104793, "Development of high-efficiency CIGS-based solar cell technology" funded by Agency for innovative development under the Ministry of higher education, science and innovation of the Republic of Uzbekistan.

Author Contributions

Damir Istamov: Conceptualization, methodology, literature review, numerical analysis, writing and revision of the manuscript. Asliddin Komilov: Supervision, scientific consultation, manuscript review and editing, and validation of the results.

Competing Interests

The authors have declared that no competing interests exist.

AI-Assisted Technologies Statement

Artificial intelligence (AI) tools were used solely for basic grammar correction and language refinement in the preparation (purpose of use) of this manuscript. Specifically, OpenAI’s ChatGPT (specific tools used) was employed to improve the readability and linguistic clarity of the English text. All scientific content, data interpretation, and conclusions were developed independently by the author. The authors have thoroughly reviewed and edited the AI-assisted text to ensure its accuracy and accept full responsibility for the content of the manuscript.

References

1. Bechlaghem S, Zebentout B, Benamara Z. The major influence of the conduction-band-offset on Zn(O, S)/$CuIn_{0.7}Ga_{0.3}Se_2$ solar cells. Results Phys. 2018; 10: 650-654.
2. Gharibzadeh S, Hossain IM, Fassl P, Nejand BA, Abzieher T, Schultes M, et al. 2D/3D heterostructure for semitransparent perovskite solar cells with engineered bandgap enables efficiencies exceeding 25% in four-terminal tandems with silicon and CIGS. Adv Funct Mater. 2020; 30: 1909919.
3. Previti F, Patanè S, Allegrini M. Polymer heterostructures with embedded carbon nanotubes for efficient photovoltaic cells. Appl Surf Sci. 2009; 255: 9877-9879.
4. Shao S, Duim H, Wang Q, Xu B, Dong J, Adjokatse S, et al. Tuning the energetic landscape of Ruddlesden-popper perovskite films for efficient solar cells. ACS Energy Lett. 2019; 5: 39-46.
5. Park NG. High efficiency perovskite solar cells: Materials and devices engineering. Trans Electr Electron Mater. 2020; 21: 1-15.
6. Zeng P, Deng W, Liu M. Recent advances of device components toward efficient flexible perovskite solar cells. Sol RRL. 2020; 4: 1900485.
7. Khattak YH, Mahmood T, Alam K, Sarwar T, Ullah I, Ullah H. Smart energy management system for utility source and photovoltaic power system using FPGA and ZigBee. Am J Electr Power Energy Syst. 2014; 3: 86-94.
8. Rimmaudo I, Salavei A, Romeo A. Effects of activation treatment on the electrical properties of low temperature grown CdTe devices. Thin Solid Films. 2013; 535: 253-256.
9. Komilov A, Abdulkhaev O, Nasrullayev Y, Abdurasulov B, Abdukahhorov B. Error minimization in PV characterization when using unfiltered light sources. Appl Sol Energy. 2024; 60: 179-188.
10. Burgelman M, Verschraegen J, Minnaert B, Marlein J. Numerical simulation of thin film solar cells: Practical exercises with SCAPS. In: Proceedings of NUMOS 2007. Ghent University & Academic Press; 2007. pp. 357-366.
11. Burgelman M, Engelhardt F, Guillemoles JF, Herberholz R, Igalson M, Klenk R, et al. Defects in Cu(In,Ga)Se_2 semiconductors and their role in the device performance of thin-film solar cells. Prog Photovoltaics Res Appl. 1997; 5: 121-130.
12. Sheplak M, Chandrasekaran V, Cain A, Nishida T, Cattafesta III LN. Characterization of a silicon-micromachined thermal shear-stress sensor. AIAA J. 2002; 40: 1099-1104.
13. Burgelman M, Marlein J. Analysis of graded band gap solar cells with SCAPS. Proceedings of the 23rd European Photovoltaic Solar Energy Conference; 2008 September 01-05; Valencia, Spain.
14. Niemegeers A, Burgelman M. Numerical modelling of ac-characteristics of CdTe and CIS solar cells. Proceedings of the Conference Record of the Twenty Fifth IEEE Photovoltaic Specialists Conference-1996; 1996 May 13-17; Washington, DC, USA. New York, NY: IEEE.
15. Burgelman M, Nollet P, Degrave S. Modelling polycrystalline semiconductor solar cells. Thin Solid Films. 2000; 361: 527-532.
16. Di Napoli S. Numerical simulation of high-efficiency CIGS-based solar cells. Parma, Italy: University of Parma; 2018.
17. Komilov A. Gallium content-dependent efficiency limits of CIGS solar cells at AM1.5G solar irradiance. J Photonics Energy. 2021; 11: 035501.

18. Goffard J, Cattoni A, Mollica F, Jubault M, Colin C, Guillemoles JF, et al. Multi-resonant light trapping in ultrathin CIGS solar cells. Proceedings of the 2016 IEEE 43rd Photovoltaic Specialists Conference (PVSC); 2016 June 05-10; Portland, OR, USA. New York, NY: IEEE.
19. Friedlmeier TM, Jackson P, Bauer A, Hariskos D, Kiowski O, Wuerz R, et al. Improved photocurrent in Cu(In,Ga)Se_2 solar cells: From 20.8% to 21.7% efficiency with CdS buffer and 21.0% Cd-free. IEEE J Photovolt. 2015; 5: 1487-1491.
20. Boukortt N, Hadri B. Bifacial *n*-PERC solar cell characterization. Indian J Phys. 2019; 93: 33-39.
21. Ghorbani T, Zahedifar M, Moradi M, Ghanbari E. Influence of affinity, band gap and ambient temperature on the efficiency of CIGS solar cells. Optik. 2020; 223: 165541.
22. Violas AF, Oliveira AJ, Teixeira JP, Lopes TS, Barbosa JR, Fernandes PA, et al. Will ultrathin CIGS solar cells overtake the champion thin-film cells? Updated SCAPS baseline models reveal main differences between ultrathin and standard CIGS. Sol Energy Mater Sol Cells. 2022; 243: 111792.
23. Kakade A, Chavan KB, Chaure S, Chaure NB. The role of window layers on the simulated performance of CIGS solar cell characteristics using SCAPS-1D. Next Res. 2025; 2: 100334.
24. Kumar A, Goyal AK, Gupta U, Gupta N, Chaujar R. Increased efficiency of 23% for CIGS solar cell by using ITO as front contact. Mater Today Proc. 2020; 28: 361-365.
25. Lundberg O, Bodegård M, Malmström J, Stolt L. Influence of the Cu(In,Ga)Se_2 thickness and Ga grading on solar cell performance. Prog Photovoltaics Res Appl. 2003; 11: 77-88.
26. Ramanathan K, Noufi R, To B, Young DL, Bhattacharya R, Contreras MA, et al. Processing and properties of sub-micron CIGS solar cells. Proceedings of the 2006 IEEE 4th World Conference on Photovoltaic Energy Conversion, WCPEC-4; 2016 May 07-12; Waikoloa, HI, USA. New York, NY: IEEE.
27. Deo M, Chauhan RK. Tweaking the performance of thin film CIGS solar cell using InP as buffer layer. Optik. 2023; 273: 170357.
28. Boukortt NE, Patanè S, Abdulraheem YM. Numerical investigation of CIGS thin-film solar cells. Sol Energy. 2020; 204: 440-447.
29. Dakua PK, Sreevedha R, Sai YA, Sri Likitha PK, Jamalbe S. Highly efficient CIGS-based solar cell with different back contact materials using SCAPS 1-D framework. J Opt. 2025; 54: 2275-2288.
30. Rahman MF, Chowdhury M, Marasamy L, Mohammed MK, Haque MD, Al Ahmed SR, et al. Improving the efficiency of a CIGS solar cell to above 31% with Sb_2S_3 as a new BSF: A numerical simulation approach by SCAPS-1D. RSC Adv. 2024; 14: 1924-1938.
31. Jayan KD, Bhattarai S. High-efficiency tandem perovskite-CIGS solar cells: Dual absorber top sub cell with $MAGeI_3$ and $Cs_2AgBiBr_6$ for enhanced photovoltaic performance. Inorg Chem Commun. 2025; 180: 114991.
32. Hajji M, Akkari A, Charrada G, Garcia-Loureiro A, Kamoun N. Improving CIGS solar cell efficiency through single, double, and triple junction absorber layer design innovations. Ceram Int. 2025; 51: 25426-25436.
33. Boukortt NE. Numerical optimization of 0.5-µm-thick Cu($In_{1-x}Ga_x$)Se_2 solar cell. Optik. 2020; 200: 163409.
34. Boukortt NE, Patanè S, AlAmri AM, AlAjmi D, Bulayyan K, AlMutairi N. Numerical investigation of perovskite and u-CIGS based tandem solar cells using silvaco TCAD simulation. Silicon. 2023; 15: 293-303.

35. Zein W, Alanazi TI, Saeed A, Salah MM, Mousa M. Proposal and design of organic/CIGS tandem solar cell: Unveiling optoelectronic approaches for enhanced photovoltaic performance. Optik. 2024; 302: 171719.
36. Chargui T, Lmai F, Mohamed AH, Bajjou O, Rahmani K. Experimental and numerical study of the CIGS/CdS heterojunction solar cell. Opt Mater. 2023; 140: 113849.
37. Houmomou AM, Nya FT, Kenfack GM, Laref A, Mohamadou A. High-performance CIGS solar cells using a double active layers approach–SCAPS 1D optoelectronic modeling approach. Inorg Chem Commun. 2024; 170: 113426.
38. Uddin MS, Hosen R, Sikder S, Mamur H, Bhuiyan MR. Photovoltaic performance enhancement of Al/ZnO:Al/i-ZnO/CdS/CIGS/Pt solar cell using SCAPS-1D software. Next Energy. 2024; 2: 100080.
39. Sikder S, Hasan MK, Mamur H, Bhuiyan MR. Optimizing layer configuration and material selection to enhance CIGS solar cell performance through computational simulation. Hybrid Adv. 2025; 10: 100460.
40. Nakamura M, Yamaguchi K, Kimoto Y, Yasaki Y, Kato T, Sugimoto H. Cd-free Cu(In,Ga)(Se,S)$_2$ thin-film solar cell with record efficiency of 23.35%. IEEE J Photovolt. 2019; 9: 1863-1867.
41. Salem M, Salah MM, Shaker A, Abouelatta M, Al-Dhlan KA, Alshammari MT, et al. A simulation-based comparative study of 2T and 4T perovskite/CIGS tandem solar cell configurations. Results Opt. 2025; 22: 100951.
42. Selmane N, Cheknane A, Khemloul F, Helal MH, Hilal HS. Cost-saving and performance-enhancement of CuInGaSe solar cells by adding CuZnSnSe as a second absorber. Sol Energy. 2022; 234: 64-80.
43. Schubbert C, Eraerds P, Richter M, Parisi J, Riedel I, Dalibor T, et al. Performance ratio study based on a device simulation of a 2D monolithic interconnected Cu(In,Ga)(Se,S)$_2$ solar cell. Sol Energy Mater Sol Cells. 2016; 157: 146-153.
44. Vidal Lorbada R, Walter T, Fuertes Marrón D, Lavrenko T, Muecke D. A deep insight into the electronic properties of CIGS modules with monolithic interconnects based on 2D simulations with TCAD. Coatings. 2019; 9: 128.
45. Lauwaert J. Back contact based T-CAD model for the N1-signal observed in capacitance spectroscopy in CIGS solar cells. Sol Energy. 2024; 273: 112506.
46. Huang CY, Parashar P, Chou HM, Lin YS, Lin A. A path-finding toward high-efficiency penternary Cu(In,Ga)(Se,S)$_2$ thin film solar module. Optik. 2019; 179: 837-847.
47. Violas AF, Oliveira AJ, Fernandes PA, Salomé PM, Teixeira JP. CIGS bifacial solar cells with novel rear architectures: Simulation point of view and the creation of a digital twin. Sol Energy Mater Sol Cells. 2024; 272: 112899.
48. Richter M, Schubbert C, Eraerds P, Parisi J, Riedel I, Dalibor T, et al. Comprehensive simulation model for Cu(In,Ga)(Se,S)$_2$ solar cells. Sol Energy Mater Sol Cells. 2015; 132: 162-171.
49. López Salas JF. Modeling and simulation of charge carrier recombination dynamics in Cu(In,Ga)Se$_2$ thin-film solar cells. Oldenburg, Germany: Universität Oldenburg; 1990.